Slew/Translation Positioning and Swing Suppression for 4-DOF Tower Cranes With Parametric Uncertainties: Design and Hardware Experimentation

Ning Sun, *Member, IEEE*, Yongchun Fang, *Senior Member, IEEE*, He Chen, Biao Lu, and Yiming Fu

***Abstract*—As a powerful large-scale construction tool, a tower crane is a strongly nonlinear underactuated system presenting complicated dynamical characteristics. Existing control methods for tower cranes are developed on the basis of simplified (i.e., linearized/approximated) crane dynamics, and most of them require exact model knowledge. However, practical tower cranes usually suffer from uncertainties (e.g., unknown rope length and payload mass); moreover, when the state variables are not close enough to the equilibrium point due to unexpected disturbances, simplified models might not reflect the actual dynamics any longer, which usually badly degrades the control performance. To tackle these problems, this paper proposes an adaptive control scheme for underactuated tower cranes to achieve simultaneous slew/translation positioning and swing suppression, which can reduce unexpected overshoots for the jib/trolley movements. The closed-loop stability is backed up with the rigorous mathematical analysis. To the best of our knowledge, the proposed controller is the *first* method for *tower cranes* with parametric uncertainties, which is developed *without* linearizing/approximating their nonlinear dynamics. Finally, we introduce our self-built multifunctional hardware crane experiment testbed and present experimental studies for the proposed method. Experimental results show that the new control approach is effective and admits satisfactory robustness.**

***Index Terms*—Nonlinear systems, tower cranes, underactuated systems, vibration/swing suppression.**

I. Introduction

FOR decades, cranes have been widely utilized and play dominant roles as powerful transportation tools in many fields, which, based on their dynamical properties, can be classified into three types, i.e., tower cranes, rotary cranes, and overhead cranes [1]. Though they have different mechanical structures and working principles, the common nature they share is that there are less independent actuators than the degrees of freedom (DOFs) that need to be controlled. Hence, analogous to many mechanical systems such as nonholonomic systems [2], [3], mobile robots [4], aerial/underwater vehicles [5]–[7], wheeled pendulum robots [8], underactuated robots [9]–[11], moving liquid containers [12], and so on, cranes are underactuated systems whose control issues are challenging and remain open.

Among different types of cranes, tower cranes have been playing indispensable roles in construction sites for putting up tall buildings (skyscrapers). Like other mechanical systems [13], vibration/suppression control is a preliminary task for cranes. At present, almost all tower cranes employed in practical environments are still manually manipulated by human operators, which presents many drawbacks, e.g., long training time required, unsatisfactory control accuracy, low working efficiency, high safety risks, and so on. With the development of mechatronics and advanced control technology, it has turned out to be an urgent practical demand to solve the slew/translation positioning and swing suppression problem for 4-DOF underactuated tower cranes, by means of developing effective control schemes.

During the past several decades, many researchers have laid their focuses on dealing with the control problem of overhead crane systems with a lot of ambitious and meaningful works reported in the literature. Based upon the fact whether or not the developed methods require realtime state feedback to generate the control commands, one may roughly partitioned them into two categories, i.e., open-loop controllers and closed-loop feedback controllers. Traditionally, for open-loop control methods, the control commands are predefined trolley acceleration reference trajectories, which are planned by utilizing the trolley translation/payload swing coupling; see, e.g., input shaping [14], [15] and trajectory planning [16]. As the trolley follows the planned reference trajectories, the trolley motion-induced swing will be reduced, and the trolley can move toward the target location at the same time. However, when uncertainties are present or the state variables are drifted from the predefined reference trajectories due to unexpected extraneous perturbations, the performance of open-loop control methods might be influenced. In order to surmount these unfavorable factors, some closed-loop feedback control methods, including nested saturation control [17], sliding mode control [18]–[20], nonlinear coupling control

Manuscript received September 24, 2015; revised January 31, 2016 and March 13, 2016; accepted March 31, 2016. Date of publication July 7, 2016; date of current version September 9, 2016. This work was supported in part by the National Natural Science Foundation of China under Grant 61503200 and Grant 61325017 and in part by the Natural Science Foundation of Tianjin under Grant 15JCQNJC03800. *(Corresponding author: Yongchun Fang.)*

The authors are with the Institute of Robotics and Automatic Information Systems, College of Computer and Control Engineering and the Tianjin Key Laboratory of Intelligent Robotics, Nankai University, Tianjin 300353, China (e-mail: sunn@nankai.edu.cn; fangyc@nankai.edu.cn; chenh@mail.nankai.edu.cn; lubiao@mail.nankai.edu.cn; fuym@mail.nankai.edu.cn).

Color versions of one or more of the figures in this paper are available online at http://ieeexplore.ieee.org.

Digital Object Identifier 10.1109/TIE.2016.2587249

[21]–[24], partial feedback linearization control [25], [26], linear control [27]–[29], adaptive control [30]–[32], observer-based control [33], [34], fuzzy logic-based control [35]–[37], genetic algorithm-based control [38], etc., are designed and applied to tackle the antiswing problem for overhead cranes.

For 4-DOF tower cranes, their dynamics are underactuated, complicated, and highly nonlinear with strong state coupling, and these factors make it challenging to conduct controller design and stability analysis, especially when *not* linearizing the nonlinear dynamics around the equilibrium point or neglecting some highly nonlinear terms. In particular, compared with overhead cranes (where only translation motion is involved), tower cranes additionally involve slew movement which produces the complex centrifugal force and inertia force (the inertia force direction is always changing). Hence, tower crane systems have more complicated dynamical characteristics than overhead cranes, and it is more difficult and challenging to achieve the dual control objectives of slew/translation positioning and swing elimination for tower cranes.

So far, there are much *fewer* available control methods reported for tower cranes than overhead cranes, since the complicated nonlinear dynamics are cumbersome to analyze for controller development. In [39], the dynamical response of underactuated tower cranes, which is coupled with payload swing motion, is thoroughly analyzed based on a linearized model. To minimize payload swing, Omar and Nayfeh develop scheduling feedback-based control schemes for tower crane systems [40], [41]. In [42], Lee *et al.* develop a laser-based path tracking system for tower cranes and validate its effectiveness. In [43], command shaping-based control approaches are developed and utilized to reduce the payload oscillations of tower cranes, by means of shaping the reference commands according to the system natural frequencies; interested readers are recommended to [44] and[45] for more details about command shaping and its applications. By simplifying the crane dynamics with small angle and slow slew/translation assumptions, an optimal velocity controller is proposed by utilizing Pontryagin's maximum principle in [46] to achieve antiswing control for tower cranes. In [47], a novel model predictive control approach is presented, by neglecting some specific terms within the tower crane dynamics, to make the payload follow a predefined path so as to fulfill the control task. Besides those model-based control approaches, Duong *et al.* design a recurrent neural network-based control strategy for underactuated tower crane systems, where a hybrid evolutionary algorithm is utilized to further improve the overall control performance [48].

After carefully summarizing the existing approaches for tower cranes, the following issues need to be solved or require further improvements.

1) Existing tower crane controllers are designed and analyzed based upon simplified (linearized/approximated) tower crane dynamics. Once the state variables are not close enough to the equilibrium point (e.g., due to unexpected disturbances), there will be significant differences between the simplified models and the real dynamics, which then influences the control performance and even leads to instability.
2) Most existing controllers require exact model knowledge (EMK), that is, they involve system parameters (e.g., rope length, trolley/payload masses, jib moment of inertia). However, the exact values of these parameters are usually difficult to obtain in practice. Moreover, the system suffers from the effects of uncertain frictions. These uncertain factors will degrade the performance of EMK-based control approaches.
3) For existing *closed-loop* tower crane controllers, there is no theoretical guarantee for reducing overshoots since merely asymptotic stability results can be achieved. Once the control parameters are not well chosen, there will be obvious overshoots not only influencing the entire efficiency but also causing unnecessary energy consumption.

In this paper, we present a new adaptive control scheme for underactuated 4-DOF tower crane systems, which can achieve superior control performance in the presence of uncertainties and reduce unexpected overshoots. Specifically, by carefully analyzing the system energy storage function, an adaptive control scheme is developed by incorporating some elaborately constructed terms to improve the transient control performance as well as to reduce unexpected overshoots for the jib slew and trolley translation movements. Then, Lyapunov-based analysis is carried out to prove the performance of the designed control scheme. Finally, we introduce a multifunctional crane experiment testbed designed and built by our research group on which we implement extensive experiments to examine the effectiveness and robustness of the proposed control method and compare it with the two existing approaches.

The originality of this paper is as follows.

1) For underactuated tower cranes, this paper derives the *first* control scheme which is designed *without* linearizing the tower crane's nonlinear dynamical equations or neglecting partial nonlinear terms. Moreover, we provide a complete rigorous theoretical closed-loop stability analysis *without* linearizing or approximating the nonlinear dynamics, either. One benefit is that, even when the state variables are not close enough to the equilibrium point, the controller can still perform satisfactorily.
2) The designed controller does *not* need the exact values of the system parameters (e.g., trolley/payload masses, rope length, jib moment of inertia), and it can increase the transient performance (in terms of swing suppression and elimination) and reduce unexpected overshoots.
3) We develop and build a hardware tower crane testbed and include experimental results to verify that the proposed control scheme achieves better control performance than the existing comparative methods and exhibits good robustness to uncertainties and extraneous disturbances.

We arrange the remaining parts as follows. In Section II, we introduce the nonlinear dynamics of underactuated tower cranes and describe the control objective mathematically. Then, the detailed controller design procedures are provided in Section III. Further, Section IV presents the stability analysis. After that the proposed controller is experimentally examined in Section V. Finally, the paper is wrapped up with conclusions in Section VI.

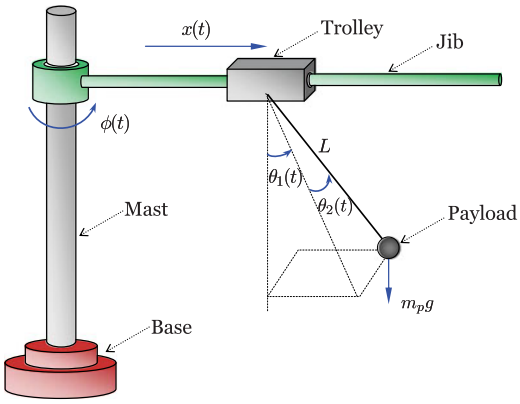

Fig. 1. Model of an underactuated tower crane system.

II. Problem Formulation

This section will provide the dynamical equations of motion for tower cranes and then give the control objective.

A. Dynamics of Tower Cranes

The dynamical equations for an underactuated 4-DOF tower crane system are as follows (see Fig. 1)[1]:

$$\begin{aligned}
&\Big[m_p\left(\sin^2\theta_1\cos^2\theta_2+\sin^2\theta_2\right)L^2+2m_pxL\cos\theta_2\sin\theta_1+J\\
&\quad+\left(m_p+m_t\right)x^2\Big]\ddot{\phi}-m_pL\sin\theta_2\ddot{x}-m_pL^2\cos\theta_1\\
&\quad\times\cos\theta_2\sin\theta_2\ddot{\theta}_1\\
&\quad+m_pL\left(\cos\theta_2x+L\sin\theta_1\right)\ddot{\theta}_2+2\left(m_p+m_t\right)x\dot{x}\dot{\phi}\\
&\quad+2m_pL\cos\theta_1\cos\theta_2x\dot{\phi}\dot{\theta}_1-m_pL\sin\theta_2(2\dot{\phi}\sin\theta_1+\dot{\theta}_2)x\dot{\theta}_2\\
&\quad+2m_pL\sin\theta_1\cos\theta_2\dot{x}\dot{\phi}+m_pL^2\sin\left(2\theta_1\right)\cos^2\theta_2\dot{\phi}\dot{\theta}_1\\
&\quad+m_pL^2\sin\theta_1\sin\theta_2\cos\theta_2\dot{\theta}_1^2+m_pL^2\cos^2\theta_1\sin(2\theta_2)\dot{\phi}\dot{\theta}_2\\
&\quad+2m_pL^2\cos\theta_1\sin^2\theta_2\dot{\theta}_1\dot{\theta}_2=M-M_f \qquad (1)\\
&-m_pL\sin\theta_2\ddot{\phi}+\left(m_p+m_t\right)\ddot{x}+m_pL\cos\theta_1\cos\theta_2\ddot{\theta}_1\\
&-m_pL\sin\theta_1\sin\theta_2\ddot{\theta}_2-\left(m_p+m_t\right)x\dot{\phi}^2-2m_pL\cos\theta_1\\
&\quad\times\sin\theta_2\dot{\theta}_1\dot{\theta}_2\\
&-m_pL\cos\theta_2\left[\sin\theta_1(\dot{\phi}^2+\dot{\theta}_1^2+\dot{\theta}_2^2)+2\dot{\phi}\dot{\theta}_2\right]=F-F_f \qquad (2)\\
&-m_pL^2\cos\theta_1\cos\theta_2\sin\theta_2\ddot{\phi}+m_pL\cos\theta_1\cos\theta_2\ddot{x}+m_pL^2\cos^2\theta_2\\
&\cdot\ddot{\theta}_1-m_pL\cos\theta_1\cos\theta_2(x+L\sin\theta_1\cos\theta_2)\dot{\phi}^2-2m_pL^2\cos\theta_2\\
&\cdot(\dot{\phi}\cos\theta_1\cos\theta_2+\dot{\theta}_1\sin\theta_2)\dot{\theta}_2+m_pgL\sin\theta_1\cos\theta_2=0 \qquad (3)\\
&m_pL(\cos\theta_2x+L\sin\theta_1)\ddot{\phi}-m_pL\sin\theta_1\sin\theta_2\ddot{x}+m_pL^2\ddot{\theta}_2\\
&+2m_pL\cos\theta_2\dot{x}\dot{\phi}+m_pL(x\sin\theta_1\sin\theta_2-L\cos^2\theta_1\sin\theta_2\cos\theta_2)\\
&\cdot\dot{\phi}^2+2m_pL^2\cos\theta_1\cos^2\theta_2\dot{\phi}\dot{\theta}_1+m_pL^2\dot{\theta}_1^2\sin\theta_2\cos\theta_2\\
&+m_pgL\cos\theta_1\sin\theta_2=0 \qquad (4)
\end{aligned}$$

[1]Throughout the paper, for a time-related variable [e.g., $M(t)$], when it appears in equations, we omit the time variable "(t)" if no confusion happens, and when it appears in the text, we keep "(t)" to distinguish with the text.

where $\phi(t)$ denotes the jib slew angle, $x(t)$ denotes the trolley translation displacement, $\theta_1(t)$, $\theta_2(t)$ are used to depict the payload's swing, J denotes the moment of inertia of the jib, m_t represents the trolley mass, m_p is the payload mass, L is the suspension rope length, g is the gravitational constant, $M(t)$ denotes the slew control toque, $F(t)$ is the translation control force, and $M_f(t)$, $F_f(t)$ are the friction torque and force, respectively. After a lot of experimental measurements, we adopt the following friction models for $M_f(t)$, $F_f(t)$[2]:

$$\begin{aligned}
M_f &= M_{f1}\tanh(\xi_\phi\dot{\phi})+M_{f2}|\dot{\phi}|\dot{\phi}\\
F_f &= F_{f1}\tanh(\xi_x\dot{x})+F_{f2}|\dot{x}|\dot{x} \qquad (5)
\end{aligned}$$

where M_{f1}, F_{f1}, M_{f2}, F_{f2}, ξ_ϕ, $\xi_x\in\mathbb{R}$ are friction-related parameters. ξ_ϕ, ξ_x hardly vary for different payload masses and, hence, can be determined offline and regarded to be *a priori* known [16]. Without loss of generality, the initial trolley horizontal displacement and jib slew angle are taken as zero, i.e.,

$$\phi(0)=0,\ x(0)=0. \qquad (6)$$

The dynamical equations (3) and (4) reflect the internal coupling that exists between the actuated trolley/jib motion and the nonactuated payload swing motion, and the mere way to eliminate the payload swing is to make full use of this coupling relationship by applying a proper feedback controller.

For crane systems working in practice, the payload is always beneath the jib. Therefore, as widely done in the crane-related literature [14]–[48], the following reasonable assumption is made:

Assumption 1: The payload swing angles satisfy $-\pi/2<\theta_1(t)<\pi/2$, $-\pi/2<\theta_2(t)<\pi/2$.

B. Control Objective

The ultimate control objective is to transfer the payload from its initial position toward the target location accurately while sufficiently suppressing and eliminating the unexpected payload swing motion, in the *presence* of parametric uncertainties. Nevertheless, due to the underactuation nature, the payload is nonactuated and cannot be *directly* controlled.

To resolve the above-mentioned issue, we alternatively decompose the control objective into two subtasks as follows:

1) make the jib arrive at its target angular position ϕ_d and drive the trolley to reach its target position x_d, which can be mathematically described as follows:

$$\lim_{t\to\infty}\phi(t)=\phi_d,\ \lim_{t\to\infty}x(t)=x_d$$

2) at the same time, suppress and eliminate the swing of the payload in the sense that

$$\lim_{t\to\infty}\theta_1(t)=0,\ \lim_{t\to\infty}\theta_2(t)=0.$$

Then, the control task is transformed into designing a suitable control scheme, *without* linearizing or approximating the

[2]As suggested in [49]–[51], disturbance observers can be used to effectively eliminate the effects of frictions. Different from that we utilize a model-based adaptive scheme to compensate for the uncertain friction force/torque, since the friction structure has been determined except for the unknown parameters.

complicated nonlinear tower crane dynamics, to achieve the above-mentioned two points in the presence of parametric uncertainties.

To be concise, the abbreviations $S_1 \triangleq \sin\theta_1$, $S_2 \triangleq \sin\theta_2$, $C_1 \triangleq \cos\theta_1, C_2 \triangleq \cos\theta_2$ will be used in the subsequent context unless otherwise claimed.

III. Controller Development

The total energy of the tower crane system is as follows:

$$E = \frac{1}{2}\dot{\boldsymbol{q}}^\top M_T(\boldsymbol{q})\dot{\boldsymbol{q}} + m_p g L(1 - C_1 C_2) \tag{7}$$

where $\boldsymbol{q} \triangleq [\ \phi \quad x \quad \theta_1 \quad \theta_2\ ]^\top$ and $M_T(\boldsymbol{q}) \in \mathbb{R}^{4\times 4}$ denotes the following positive-definite symmetric matrix:

$$M_T(\boldsymbol{q}) = \begin{bmatrix} m_{11} & m_{12} & m_{13} & m_{14} \\ m_{12} & m_p + m_t & m_p L C_1 C_2 & -m_p L S_1 S_2 \\ m_{13} & m_p L C_1 C_2 & m_p L^2 C_2^2 & 0 \\ m_{14} & -m_p L S_1 S_2 & 0 & m_p L^2 \end{bmatrix}$$

with

$$\begin{aligned} m_{11} &\triangleq\ m_p L^2(S_1^2 C_2^2 + S_2^2) + 2 m_p L x S_1 C_2 + (m_p + m_t)x^2 + J \\ m_{12} &\triangleq -m_p L S_2,\ m_{13} \triangleq -m_p L^2 C_1 S_2 C_2 \\ m_{14} &\triangleq\ m_p L(C_2 x + L S_1). \end{aligned} \tag{8}$$

Then, we can take the time derivative of $E(t)$, insert for (1)–(4), and make tedious mathematical operations to obtain

$$\dot{E} = (M - M_f)\dot{\phi} + (F - F_f)\dot{x} \tag{9}$$

implying that the tower crane system is passive. It is also inferred from (9) that the energy can merely be eliminated via the actuated jib and trolley motion, i.e., $\dot{\phi}(t)$ and $\dot{x}(t)$.

Further, in view of (5), one can rewrite (9) into

$$\dot{E} = (M - \boldsymbol{\eta}_\phi^\top \boldsymbol{\omega}_\phi)\dot{\phi} + (F - \boldsymbol{\eta}_x^\top \boldsymbol{\omega}_x)\dot{x} \tag{10}$$

where the vectors $\boldsymbol{\eta}_\phi,\ \boldsymbol{\eta}_x,\ \boldsymbol{\omega}_\phi,\ \boldsymbol{\omega}_x \in \mathbb{R}^2$ are defined as

$$\begin{aligned} \boldsymbol{\eta}_\phi &\triangleq\ [\tanh(\xi_\phi \dot{\phi}) \quad |\dot{\phi}|\dot{\phi}]^\top,\ \boldsymbol{\omega}_\phi \triangleq [M_{f1} \quad M_{f2}]^\top \\ \boldsymbol{\eta}_x &\triangleq\ [\tanh(\xi_x \dot{x}) \quad |\dot{x}|\dot{x}]^\top,\ \boldsymbol{\omega}_x \triangleq [F_{f1} \quad F_{f2}]^\top. \end{aligned} \tag{11}$$

Next, we will design an adaptive control scheme, which does not involve system parameter-related terms, for tower crane systems.

At first, let the following error signals be introduced:

$$e_\phi = \phi - \phi_d,\ e_x = x - x_d \Longrightarrow \dot{e}_\phi = \dot{\phi},\ \dot{e}_x = \dot{x}. \tag{12}$$

After that to incorporate the control objective into the controller design, we further construct the following continuous differentiable positive definite scalar function $W(t)$ on the basis of (7):

$$\begin{aligned} W \triangleq \frac{1}{2}\dot{\boldsymbol{q}}^\top M_T(\boldsymbol{q})\dot{\boldsymbol{q}} + m_p g L(1 - C_1 C_2) + \frac{1}{2}k_{p\phi} e_\phi^2 + \frac{1}{2}k_{px} e_x^2 \\ + \frac{1}{2}\tilde{\boldsymbol{\omega}}_\phi^\top \Pi_\phi^{-1}\tilde{\boldsymbol{\omega}}_\phi + \frac{1}{2}\tilde{\boldsymbol{\omega}}_x^\top \Pi_x^{-1}\tilde{\boldsymbol{\omega}}_x \end{aligned} \tag{13}$$

where $k_{p\phi},\ k_{px} \in \mathbb{R}^+$ are positive control gains to be introduced later, $\tilde{\boldsymbol{\omega}}_\phi(t),\ \tilde{\boldsymbol{\omega}}_x(t) \in \mathbb{R}^2$ are estimation error vectors defined by

$$\tilde{\boldsymbol{\omega}}_\phi = \hat{\boldsymbol{\omega}}_\phi - \boldsymbol{\omega}_\phi,\ \tilde{\boldsymbol{\omega}}_x = \hat{\boldsymbol{\omega}}_x - \boldsymbol{\omega}_x \Longrightarrow \dot{\tilde{\boldsymbol{\omega}}}_\phi = \dot{\hat{\boldsymbol{\omega}}}_\phi,\ \dot{\tilde{\boldsymbol{\omega}}}_x = \dot{\hat{\boldsymbol{\omega}}}_x \tag{14}$$

with $\hat{\boldsymbol{\omega}}_\phi(t),\ \hat{\boldsymbol{\omega}}_x(t) \in \mathbb{R}^2$ being the online estimated signals for $\boldsymbol{\omega}_\phi,\ \boldsymbol{\omega}_x$ [see (11)], respectively, i.e.,

$$\hat{\boldsymbol{\omega}}_\phi \triangleq [\hat{M}_{f1} \quad \hat{M}_{f2}]^\top,\ \hat{\boldsymbol{\omega}}_x \triangleq [\hat{F}_{f1} \quad \hat{F}_{f2}]^\top \tag{15}$$

and $\Pi_\phi = \mathrm{diag}\{\pi_{\phi 1}, \pi_{\phi 2}\} \in \mathbb{R}^{2\times 2}$, $\Pi_x = \mathrm{diag}\{\pi_{x1}, \pi_{x2}\} \in \mathbb{R}^{2\times 2}$ are positive definite matrices to be introduced later with $\pi_{\phi 1},\ \pi_{\phi 2},\ \pi_{x1},\ \pi_{x2} \in \mathbb{R}^+$ being positive tunable update gains. After differentiating (13) with respect to time, inserting for (1)–(4) and (10), and implementing some tedious mathematical manipulations, we can obtain the following result:

$$\begin{aligned} \dot{W} = (M + k_{p\phi} e_\phi - \boldsymbol{\eta}_\phi^\top \boldsymbol{\omega}_\phi)\dot{\phi} + (F + k_{px} e_x - \boldsymbol{\eta}_x^\top \boldsymbol{\omega}_x)\dot{x} \\ + \tilde{\boldsymbol{\omega}}_\phi^\top \Pi_\phi^{-1}\dot{\hat{\boldsymbol{\omega}}}_\phi + \tilde{\boldsymbol{\omega}}_x^\top \Pi_x^{-1}\dot{\hat{\boldsymbol{\omega}}}_x \end{aligned} \tag{16}$$

where (14) is used. Then, based on the form of (16), as a means to cancel the crossing terms and render $\dot{W}(t)$ nonpositive, we first give the following preliminary control law:

$$\begin{aligned} M_{bc} &= -k_{p\phi} e_\phi - k_{d\phi}\dot{\phi} + \boldsymbol{\eta}_\phi^\top \hat{\boldsymbol{\omega}}_\phi \\ F_{bc} &= -k_{px} e_x - k_{dx}\dot{x} + \boldsymbol{\eta}_x^\top \hat{\boldsymbol{\omega}}_x \end{aligned} \tag{17}$$

where $k_{d\phi},\ k_{dx} \in \mathbb{R}^+$ are positive control gains and the update law for $\hat{\boldsymbol{\omega}}_\phi(t),\ \hat{\boldsymbol{\omega}}_x(t)$ is designed as follows:

$$\dot{\hat{\boldsymbol{\omega}}}_\phi = -\Pi_\phi \boldsymbol{\eta}_\phi \dot{\phi},\ \dot{\hat{\boldsymbol{\omega}}}_x = -\Pi_x \boldsymbol{\eta}_x \dot{x}. \tag{18}$$

Inserting (17) and (18) into (16) yields

$$\dot{W} = -k_{d\phi}\dot{\phi}^2 - k_{dx}\dot{x}^2 \le 0 \tag{19}$$

indicating that (13) *merely* vanishes along the actuated state variables $\dot{\phi}(t)$ and $\dot{x}(t)$, which is due to the underactuated nature.

Although we can prove that the closed-loop equilibrium point is asymptotically stable by using (17), the useful nonactuated swing-related information is not directly used. On the other hand, one common issue associated with most feedback control methods [including (17)] is the probable presence of overshoots.

To overcome the above-mentioned drawbacks, we present the final adaptive controller as follows:

$$\begin{aligned} M_{ic} = &-\frac{\beta_\phi\left[(\phi_d + \varepsilon_\phi)^2 - \phi^2 + \phi e_\phi\right]}{\left[(\phi_d + \varepsilon_\phi)^2 - \phi^2\right]^2} e_\phi - k_{h\phi}(\dot{\theta}_1^2 + \dot{\theta}_2^2)\dot{\phi} \\ &-k_{p\phi} e_\phi - k_{d\phi}\dot{\phi} + \boldsymbol{\eta}_\phi^\top \hat{\boldsymbol{\omega}}_\phi \\ F_{ic} = &-\frac{\beta_x\left[(x_d + \varepsilon_x)^2 - x^2 + x e_x\right]}{\left[(x_d + \varepsilon_x)^2 - x^2\right]^2} e_x - k_{hx}(\dot{\theta}_1^2 + \dot{\theta}_2^2)\dot{x} \\ &-k_{px} e_x - k_{dx}\dot{x} + \boldsymbol{\eta}_x^\top \hat{\boldsymbol{\omega}}_x \end{aligned} \tag{20}$$

where $k_{h\phi},\ k_{hx},\ \beta_\phi,\ \beta_x \in \mathbb{R}^+$ are positive control gains, and the positive parameters ε_ϕ and $\varepsilon_x \in \mathbb{R}^+$ are introduced to restrict the maximum overshoot amplitudes for $\phi(t)$ and $x(t)$,

respectively. The designed controller (20) does not have the singularity problem, as will be proven by (26)–(28).

Remark 1: The preliminary version in (17) is the basis and a part of the final controller (20). More precisely, compared with (17), the final controller (20) contains two additional nonlinear terms, where the first terms in (20) are used to reduce the overshoots for the jib slew and trolley translation movements, and the second terms in (20) have incorporated swing-related information as a means to enhance the swing suppression and elimination control performance.

Remark 2: There is no rigorous theoretical guarantee for analyzing the overshoots of (17) [a part of the final controller (20)], whose control gains can *only* be derived via *trial and error* experimentation. The major drawback of such a tuning procedure is that we need to try many times before getting a suitable set of control gains, and in most cases, significant overshoots are present. By contrast, for the final controller (20), the overshoots have been carefully taken into consideration when we perform controller design and analysis, and the benefit is that, as long as we choose β_ϕ and β_x as nonzero, the maximum amplitudes of the overshoots will not exceed ε_ϕ and ε_x, respectively.

IV. Closed-Loop Stability Analysis

This section presents theoretical analysis for the stability of the closed-loop system's equilibrium point.

Theorem 1: The designed controller (20), along with the update law in (18), can drive the actuated variables [i.e., the jib slew angle $\phi(t)$ and the trolley displacement $x(t)$] to reach their desired positions, respectively, and simultaneously suppress/eliminate the nonactuated payload angles $\theta_1(t)$ and $\theta_2(t)$. In addition, during the overall process, the slew angle $\phi(t)$ and the trolley displacement $x(t)$ never exceed $\phi_d+\varepsilon_\phi$ and $x_d+\varepsilon_x$, respectively. In other words, the overshoots for $\phi(t)$ and $x(t)$ are less than ε_ϕ and ε_x, respectively. These conclusions can be mathematically described as follows:

$$\begin{aligned}&\lim_{t\to\infty}\left[\begin{array}{cccc}\phi(t) & x(t) & \dot\phi(t) & \dot x(t)\end{array}\right]^\top=\left[\begin{array}{cccc}\phi_d & x_d & 0 & 0\end{array}\right]^\top\\&\lim_{t\to\infty}\left[\begin{array}{cccc}\theta_1(t) & \theta_2(t) & \dot\theta_1(t) & \dot\theta_2(t)\end{array}\right]^\top=\left[\begin{array}{cccc}0 & 0 & 0 & 0\end{array}\right]^\top\\&\phi(t)<\phi_d+\varepsilon_\phi,\ x(t)<x_d+\varepsilon_x\end{aligned}\tag{21}$$

where ε_ϕ and ε_x are defined below (20).

Proof: To begin with let the following scalar function $V(t)$ be constructed:

$$\begin{aligned}V\triangleq\ &\frac{1}{2}\dot{\boldsymbol{q}}^\top M_T(\boldsymbol{q})\dot{\boldsymbol{q}}+m_pgL(1-C_1C_2)+\frac{1}{2}k_{p\phi}e_\phi^2+\frac{1}{2}k_{px}e_x^2\\&+\frac{\beta_\phi e_\phi^2}{2\left[(\phi_d+\varepsilon_\phi)^2-\phi^2\right]}+\frac{\beta_x e_x^2}{2\left[(x_d+\varepsilon_x)^2-x^2\right]}\\&+\frac{1}{2}\tilde{\boldsymbol{\omega}}_\phi^\top\Pi_\phi^{-1}\tilde{\boldsymbol{\omega}}_\phi+\frac{1}{2}\tilde{\boldsymbol{\omega}}_x^\top\Pi_x^{-1}\tilde{\boldsymbol{\omega}}_x.\end{aligned}\tag{22}$$

Then, we can differentiate $V(t)$ with respect to time and insert for (10), (18), and (14) to derive the following result:

$$\begin{aligned}\dot V=\ &\left\{M+k_{p\phi}e_\phi+\frac{\beta_\phi\left[(\phi_d+\varepsilon_\phi)^2-\phi^2+\phi e_\phi\right]}{\left[(\phi_d+\varepsilon_\phi)^2-\phi^2\right]^2}e_\phi-\boldsymbol{\eta}_\phi^\top\boldsymbol{\omega}_\phi\right\}\dot\phi\\&+\left\{F+k_{px}e_x+\frac{\beta_x\left[(x_d+\varepsilon_x)^2-x^2+xe_x\right]}{\left[(x_d+\varepsilon_x)^2-x^2\right]^2}e_x-\boldsymbol{\eta}_x^\top\boldsymbol{\omega}_x\right\}\dot x\\&-\tilde{\boldsymbol{\omega}}_\phi^\top\boldsymbol{\eta}_\phi\dot\phi-\tilde{\boldsymbol{\omega}}_x^\top\boldsymbol{\eta}_x\dot x.\end{aligned}\tag{23}$$

Further, by substituting (20) into (23) and then taking advantage of (18), it can be obtained that

$$\begin{aligned}\dot V=&-k_{d\phi}\dot\phi^2-k_{dx}\dot x^2-(k_{h\phi}\dot\phi^2+k_{hx}\dot x^2)\dot\theta_1^2\\&-(k_{h\phi}\dot\phi^2+k_{hx}\dot x^2)\dot\theta_2^2\le 0\end{aligned}\tag{24}$$

which indicates that

$$V(t)\le V(0)\ll+\infty.\tag{25}$$

We can infer from (6) that $|\phi(0)|<\phi_d+\varepsilon_\phi$, $|x(0)|<x_d+\varepsilon_x$. Assuming that $\phi(t)$ [respectively, $x(t)$] tends to exceed the boundary of $|\phi(t)|<\phi_d+\varepsilon_\phi$ [respectively, $|x(t)|<x_d+\varepsilon_x$] from the interior, then it is clear from (22) that $V(t)\to+\infty$ which invalidates $V(t)\ll+\infty$ in (25). Thus, one has

$$|\phi(t)|<\phi_d+\varepsilon_\phi,\ |x(t)|<x_d+\varepsilon_x\tag{26}$$

which indicates that the overshoots of $\phi(t)$ and $x(t)$ are, respectively, less than ε_ϕ and ε_x. It is also indicated from (26) that $(\phi_d+\varepsilon_\phi)^2-\phi^2>0$ and $(x_d+\varepsilon_x)^2-x^2>0$, which further implies that $V(t)$ in (22) is always nonnegative, i.e., $V(t)\ge 0$, and it is hence a control *Lyapunov* function candidate. Then, noting that $V(0)$ is bounded, it is easy to conclude that

$$\begin{aligned}V\in\mathcal{L}_\infty\Longrightarrow\ &e_\phi,\ e_x,\ \dot\phi,\ \dot x,\ \dot\theta_1,\ \dot\theta_2,\ \tilde{\boldsymbol{\omega}}_\phi,\ \tilde{\boldsymbol{\omega}}_x,\ \hat{\boldsymbol{\omega}}_\phi,\ \hat{\boldsymbol{\omega}}_x\in\mathcal{L}_\infty,\\&\frac{e_\phi^2}{(\phi_d+\varepsilon_\phi)^2-\phi^2},\ \frac{e_x^2}{(x_d+\varepsilon_x)^2-x^2}\in\mathcal{L}_\infty.\end{aligned}\tag{27}$$

Moreover, if $e_\phi(t)\to 0$, then $\frac{1}{(\phi_d+\varepsilon_\phi)^2-\phi^2}\to\frac{1}{(\phi_d+\varepsilon_\phi)^2-\phi_d^2}\in\mathcal{L}_\infty$. In addition, if $e_\phi(t)\nrightarrow 0$, then it follows from $e_\phi(t)\in\mathcal{L}_\infty$ and $\frac{e_\phi^2}{(\phi_d+\varepsilon_\phi)^2-\phi^2}\in\mathcal{L}_\infty$ that $\frac{1}{(\phi_d+\varepsilon_\phi)^2-\phi^2}\in\mathcal{L}_\infty$. Similar analysis can be implemented for $\frac{1}{(x_d+\varepsilon_x)^2-x^2}$. Hence, it is indicated, along with (20) and (27), that

$$\frac{1}{(\phi_d+\varepsilon_\phi)^2-\phi^2},\ \frac{1}{(x_d+\varepsilon_x)^2-x^2},\ M,\ F\in\mathcal{L}_\infty.\tag{28}$$

To prove (21), we need to perform further analysis. To this end, define Ξ as the set of all the trajectories such that $\dot V(t)=0$, i.e.,

$$\Xi\triangleq\{(\boldsymbol{q},\dot{\boldsymbol{q}})\mid\dot V=0\}.\tag{29}$$

Then, we further denote Λ as the largest invariant set included in Ξ. Then, it follows from (5), (24), and (29) that, in Λ,

$$\begin{aligned}&\dot\phi=0,\ \dot x=0\Longrightarrow\ddot\phi=0,\ \ddot x=0,\ M_f=0,\ F_f=0\Longrightarrow\\&e_\phi=\lambda_1,\ e_x=\lambda_2\Longrightarrow\phi=\lambda_1+\phi_d,\ x=\lambda_2+x_d\end{aligned}\tag{30}$$

where λ_1, λ_2 are constants to be determined. Then, in the set Λ, it is known from (30) that $M(t)$ and $F(t)$ in (20) reduce to

$$M=\lambda_3,\ F=\lambda_4\tag{31}$$

where λ_3, λ_4 are constants explicitly expressed as

$$\lambda_3\triangleq-\frac{\beta_\phi\left[(\phi_d+\varepsilon_\phi)^2-(\lambda_1+\phi_d)^2+(\lambda_1+\phi_d)\lambda_1\right]}{\left[(\phi_d+\varepsilon_\phi)^2-(\lambda_1+\phi_d)^2\right]^2}\lambda_1$$

$$-k_{p\phi}\lambda_1,$$
$$\lambda_4 \triangleq -\frac{\beta_x\left[(x_d+\varepsilon_x)^2-(\lambda_2+x_d)^2+(\lambda_2+x_d)\lambda_2\right]}{\left[(x_d+\varepsilon_x)^2-(\lambda_2+x_d)^2\right]^2}\lambda_2$$
$$-k_{px}\lambda_2 \tag{32}$$

i.e., both $M(t)$ and $F(t)$ keep *constant* in Λ. We will complete the invariant-set-based analysis with two steps.

Step 1. We first prove that $e_\phi(t)=0$, $e_x(t)=0$, $F(t)=0$, $M(t)=0$ in Λ. Dividing both sides of (1) with m_pL and applying the conclusions in (30), one has the following equation:

$$-LC_1C_2S_2\ddot{\theta}_1+(\lambda_2+x_d)C_2\ddot{\theta}_2+LS_1\ddot{\theta}_2-(\lambda_2+x_d)S_2\dot{\theta}_2^2$$
$$+LS_1S_2C_2\dot{\theta}_1^2+2LC_1S_2^2\dot{\theta}_1\dot{\theta}_2=\frac{\lambda_3}{m_pL}. \tag{33}$$

To proceed, we intend to integrate both sides of (33) with respect to time; however, the left-hand side is *not* directly integrable. As a means to deal with this issue, by using the fact that $S_2^2\equiv 1-C_2^2$, one can expand $LC_1S_2^2\dot{\theta}_1\dot{\theta}_2$ in the following way:

$$LC_1S_2^2\dot{\theta}_1\dot{\theta}_2=LC_1\dot{\theta}_1\dot{\theta}_2-LC_1C_2^2\dot{\theta}_1\dot{\theta}_2. \tag{34}$$

Using (34) and performing arrangements, we rewrite (33) as

$$-LC_1C_2S_2\ddot{\theta}_1+LS_1S_2C_2\dot{\theta}_1^2+LC_1S_2^2\dot{\theta}_1\dot{\theta}_2-LC_1C_2^2\dot{\theta}_1\dot{\theta}_2$$
$$+LS_1\ddot{\theta}_2+LC_1\dot{\theta}_1\dot{\theta}_2+(\lambda_2+x_d)(C_2\ddot{\theta}_2-S_2\dot{\theta}_2^2)=\frac{\lambda_3}{m_pL}$$
$$\Longleftrightarrow \frac{\mathrm{d}}{\mathrm{d}t}\left[-LC_1S_2C_2\dot{\theta}_1+LS_1\dot{\theta}_2+(\lambda_2+x_d)C_2\dot{\theta}_2\right]=\frac{\lambda_3}{m_pL}. \tag{35}$$

The integral of (35) in time can be calculated as follows:

$$-LC_1S_2C_2\dot{\theta}_1+LS_1\dot{\theta}_2+(\lambda_2+x_d)C_2\dot{\theta}_2=\frac{\lambda_3}{m_pL}t+\lambda_5 \tag{36}$$

where λ_5 denotes a constant yet to be determined. If the constant λ_3 in (31) is *nonzero*, then as $t\to\infty$,

$$\left|-LC_1S_2C_2\dot{\theta}_1+LS_1\dot{\theta}_2+(\lambda_2+x_d)C_2\dot{\theta}_2\right|\to+\infty \tag{37}$$

which *contradicts* with the conclusions of $S_1,C_1,S_2,C_2\in\mathcal{L}_\infty$, and $\dot{\theta}_1(t),\dot{\theta}_2(t)\in\mathcal{L}_\infty$ [see (27)]. Hence, $\lambda_3=0$, which further implies from (30)–(32) and (36) that, in Λ,

$$-LC_1S_2C_2\dot{\theta}_1+LS_1\dot{\theta}_2+(\lambda_2+x_d)C_2\dot{\theta}_2=\lambda_5,\ M=0. \tag{38}$$

By employing $\phi=\lambda_1+\phi_d$ [see (30)] and $\lambda_3=0$, one can rewrite the first equation in (32), after some arrangements, as

$$\left\{k_{p\phi}+\frac{\beta_\phi\left[(\phi_d+\varepsilon_\phi)^2-\phi\phi_d\right]}{\left[(\phi_d+\varepsilon_\phi)^2-(\lambda_1+\phi_d)^2\right]^2}\right\}\lambda_1=0. \tag{39}$$

As $\phi<\phi_d+\varepsilon_\phi$ [see (26)] and $\phi_d<\phi_d+\varepsilon_\phi$, one has $(\phi_d+\varepsilon_\phi)^2>|\phi\phi_d|\geq\phi\phi_d$, indicating that the bracket term in (39) is always positive. Thus, it is known from (39) and (30) that

$$\lambda_1=0\Longrightarrow e_\phi=0,\ \phi=\phi_d. \tag{40}$$

Similar with (33), by using (30), one can reduce (2) into

$$C_1C_2\ddot{\theta}_1-S_1C_2\dot{\theta}_1^2-2C_1S_2\dot{\theta}_1\dot{\theta}_2-S_1S_2\ddot{\theta}_2-S_1C_2\dot{\theta}_2^2=\frac{\lambda_4}{m_pL}$$
$$\Longleftrightarrow \frac{\mathrm{d}}{\mathrm{d}t}\left(C_1C_2\dot{\theta}_1-S_1S_2\dot{\theta}_2\right)=\frac{\lambda_4}{m_pL}. \tag{41}$$

Then, we can integrate (41) with respect to time to yield

$$C_1C_2\dot{\theta}_1-S_1S_2\dot{\theta}_2=\frac{\lambda_4}{m_pL}t+\lambda_6 \tag{42}$$

where λ_6 is constant. Similar arguments with those in (36)–(40) can be carried out for (42) to conclude that

$$\lambda_4=0,\ F=0,\ e_x=0,\ \lambda_2=0,\ x=x_d \tag{43}$$
$$C_1C_2\dot{\theta}_1-S_1S_2\dot{\theta}_2=\lambda_6. \tag{44}$$

Step 2. We further illustrate that $\theta_1(t)=0,\theta_2(t)=0,\dot{\theta}_1(t)=0,\ \dot{\theta}_2(t)=0$ in Λ. By utilizing (30), after some arrangements, one can reduce (3) and (4) into

$$LC_2^2\ddot{\theta}_1=2LS_2C_2\dot{\theta}_1\dot{\theta}_2-gS_1C_2 \tag{45}$$
$$L\ddot{\theta}_2=-L\dot{\theta}_1^2S_2C_2-gC_1S_2. \tag{46}$$

In addition, multiplying both sides of (41) with LC_2 and using $\lambda_4=0$ [see (43)] yields

$$LC_1C_2^2\ddot{\theta}_1-LS_1C_2^2\dot{\theta}_1^2-2LC_1S_2C_2\dot{\theta}_1\dot{\theta}_2$$
$$-LS_1S_2C_2\ddot{\theta}_2-LS_1C_2^2\dot{\theta}_2^2=0. \tag{47}$$

Then, by inserting (45) and (46) into (47), canceling the common terms, and rearranging the obtained equation, we are led to

$$gS_1C_1C_2^3+LS_1C_2^4\dot{\theta}_1^2+LS_1C_2^2\dot{\theta}_2^2=0 \tag{48}$$

where we have used the triangular identity $S_2^2+C_2^2\equiv 1$. Noting that $C_2>0$ (see *Assumption 1*), one can divide both sides of (48) with C_2^2 to derive

$$S_1\left(gC_1C_2+LC_2^2\dot{\theta}_1^2+L\dot{\theta}_2^2\right)=0. \tag{49}$$

Again, using $C_1>0$, $C_2>0$ (see *Assumption 1*), the bracket term in (49) is always larger than zero. Hence, it follows from (49) that

$$S_1=0\Longrightarrow\theta_1=0\Longrightarrow\dot{\theta}_1=0,\ \ddot{\theta}_1=0 \tag{50}$$

where *Assumption 1* is used. Inserting (50) into (44) yields $\lambda_6=0$.

Further, we can use (43) and (50) to simplify (38) as

$$C_2\dot{\theta}_2=\frac{\lambda_5}{x_d}\Longrightarrow S_2=\frac{\lambda_5}{x_d}t+\lambda_7 \tag{51}$$

where λ_7 is a constant number. Again, by performing some reduction to absurdity analysis similar with those in (36) and (37), it is not difficult to show, by using $|S_2|\leq 1$, that

$$\lambda_5=0,\ S_2=\lambda_7. \tag{52}$$

It can be concluded from $\dot{\theta}_2(t) \in \mathcal{L}_\infty$ [see (27)] that $\theta_2(t)$ is uniformly continuous. Thus, it follows from (52) that $\theta_2(t)$ takes a *constant* value in Λ. Hence, in the set Λ, we always have

$$\dot{\theta}_2(t) = 0 \Longrightarrow \ddot{\theta}_2(t) = 0. \tag{53}$$

Then, substituting (50) and (53) into (46) produces

$$gC_1S_2 = 0 \tag{54}$$

which, together with $C_1 > 0$ (see *Assumption 1*), indicates that

$$S_2 = 0 \Longrightarrow \theta_2 = 0 \tag{55}$$

upon using *Assumption 1*.

After gathering the results in (26), (30), (38), (40), (43), (50), (53), and (55), the largest invariant set Λ contains only the closed-loop equilibrium point. Then, the conclusions of Theorem 1 can be proven by applying LaSalle's invariance principle [52].

Remark 3: The first terms in (20) stem from $V(t)$ given in (22). It is seen that $V(t)$ includes two nonnegative terms $\beta_\phi e_\phi^2/\{2[(\phi_d + \varepsilon_\phi)^2 - \phi^2]\}$ and $\beta_x e_x^2/\{2[(x_d + \varepsilon_x)^2 - x^2]\}$, which will tend to infinity if the overshoots of $\phi(t)$, $x(t)$ approach ε_ϕ, ε_x. Thus, the first terms in (20) are motivated to cancel the crossing terms in $\dot{V}(t)$ of (23) to prevent $V(t)$ from escaping to infinity, so that the overshoots of $\phi(t)$ and $x(t)$ can be suppressed to be less than ε_ϕ and ε_x, respectively, as shown in (26). Additionally, by comparing (19) with (24), two extra nonpositive terms $-(k_{h\phi}\dot{\phi}^2 + k_{hx}\dot{x}^2)\dot{\theta}_1^2$ and $-(k_{h\phi}\dot{\phi}^2 + k_{hx}\dot{x}^2)\dot{\theta}_2^2$ are included in (24) because of the second terms in (20). Due to the underactuated nature, the actuated and nonactuated state variables are always coupled with and influence each other, i.e., if the actuated variables vary with time, they will affect the trajectories of the nonactuated ones, and vice versa. As long as $\dot{\theta}_1(t)$, $\dot{\theta}_2(t)$ are nonzero, they will always influence $\dot{\phi}(t)$, $\dot{x}(t)$ in turn. As a result, the nonpositive "coefficient" $-(k_{h\phi}\dot{\phi}^2 + k_{hx}\dot{x}^2)$ in (24) will not be always zero until $\dot{\theta}_1(t)$ and $\dot{\theta}_2(t)$ are regulated to zero, that is, the last two terms in (24) are active before $\dot{V}(t) \equiv 0$. It is inferred from (19) that $W(t)$ *merely* vanishes along the actuated state variables; by contrast, we see from (24) that $V(t)$ vanishes along both the actuated and nonactuated state variables, which implies that the controller (20) induces further swing-related damping to accelerate swing suppression and elimination.

V. Hardware Experiments

This section exhibits hardware experimental results to verify the performance of the proposed control method.

A. Self-Built Multifunctional Crane Experiment Testbed

We first briefly describe the utilized multifunctional hardware crane experiment testbed, as shown in Fig. 2. The multifunctional crane testbed is made up of a mechanical body, actuating devices/sensors, and a computer-based control system.

1) Mechanical Body and Actuating Devices/Sensors: As illustrated in Fig. 2, the jib can rotate around the mast fixed to the base, and the trolley can move along the jib. All the movements are generated by ac motors (accompanied with reduction gears) which are controlled by servo actuators connected to the computer-based control system. The trolley translation displacement and the jib slew angle are measured by coaxial encoders embedded within the ac servo motors. The payload is suspended from the trolley through a steel rope, whose swing motion can be conveniently captured in real time by angular encoders equipped beneath the trolley. With these moving devices, we are admitted to study the dynamical characteristics of a *tower* crane system. On the other hand, the jib can also perform pitch motion so that the built crane testbed turns to a *boom* crane by fixing the trolley to some position on the jib. In addition, we have specifically designed the base in such a way that it can undulate, if needed, under the actuation of three ac servo motors, which can be utilized to imitate the effects of sea waves, and in this case, the crane testbed acts as an *offshore* crane working in the sea environment. In this paper, the crane experiment testbed is set to work in the mode of a tower crane. It is worthwhile to point out that, when the self-built testbed works as a tower crane, although its size is not large, it is carefully and elaborately designed in order to capture the dynamical characteristics of a tower crane, and it has all the functions of a tower crane, including trolley translation, jib slew, payload swing, and so forth. Additionally, we have carried out a lot of experimental tests to verify its performance, which demonstrate that it can well reflect the working principle of tower cranes.

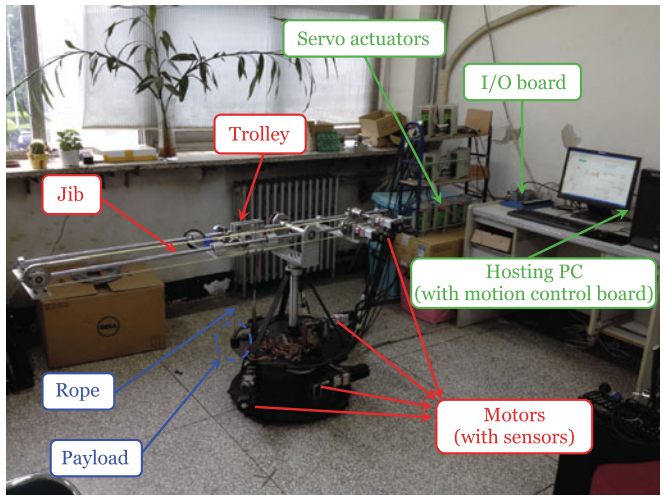

Fig. 2. Self-built multifunctional hardware crane experiment testbed.

2) Computer-Based Control System: The control system mainly consists of a hosting PC, a motion control board (embedded within the PC), and a software control system (see Fig. 2). In particular, a GTS-800-PV-PCI eight-axis motion control board made by Googol Technology Limited, together with a GT2-800-ACC2-V I/O interface board, is used to collect data from the sensors and convey them to the hosting PC in real time, and simultaneously, it outputs the control commands generated by the hosting PC to make the ac servo motors generate the corresponding actuating forces/torques. As for the software

control system, the MATLAB/Simulink 2012b Real-Time Windows Target which runs in the environment of the Windows XP operating system is used to implement the developed control approach in real time, with the control period being configured as 5 ms.

For the utilized testbed, the physical parameters, including the trolley mass and the jib moment of inertia, are set as $m_t = 3.5$ kg, $J = 6.8$ kg $\cdot$ m^2, $g = 9.8$ m/s^2. In addition, the payload mass m_p and the rope length L can be adjusted as needed. Unless otherwise mentioned, m_p and L are set as

$$m_p = 0.5 \text{ kg}, \ L = 0.5 \text{ m}. \tag{56}$$

B. Experimental Results and Analysis

In order to fully verify the actual control performance, we have carried out two groups of hardware experiments. More precisely, we compare the performance of the proposed controller with those of the robust extra-insensitive (EI) control approach [44] and the linear quadratic regulator (LQR) method in *Experiment 1*. After that, in *Experiment 2*, the performance of the proposed method is then experimentally examined in the presence of different unfavorable conditions.

For all the experiments, without loss of generality, the initial jib slew and trolley translation positions are taken as $\phi(0) = 0^\circ$ and $x(0) = 0$ m, respectively. The target jib slew and trolley translation positions are set as $\phi_d = \pi/2$ rad and $x_d = 0.4$ m, respectively. In order to guarantee soft start, as in [30], ϕ_d and x_d are changed to be $\phi_d = (\pi/2)(1 - \mathrm{e}^{-8.33t^3})$ rad and $x_d = 0.4(1 - \mathrm{e}^{-8.33t^3})$ m for implementation, respectively.

1) Experiment 1: In this group of experiments, to better show the designed controller' performance, the well-known robust EI control method in [44] and the LQR method are chosen for comparisons. For the comparative EI control approach, the tolerance level of vibration is chosen as 5% as in [44] and the natural period is calculated as $T = 1.4192$ s, which can be used to determine the control commands. Regarding the LQR method, by linearizing the tower crane dynamics around the equilibrium point, we can obtain two decoupled linear systems in state space forms. Their performance indices are chosen as $J_{\text{lqr}} = \int_0^\infty \left(X^\top Q X + RF^2\right) \mathrm{d}t$ where $X = [\phi(t) - \phi_d, \ \dot{\phi}(t) - \dot{\phi}_d, \ \theta_2(t), \ \dot{\theta}_2(t)]^\top$ for the slew subsystem and $X = [x(t) - x_d, \ \dot{x}(t) - \dot{x}_d, \ \theta_1(t), \ \dot{\theta}_1(t)]^\top$ for the translation subsystem, respectively. After careful tuning, we choose two sets of Q and R as $Q = \text{diag}\{10, 14, 150, 0\}$, $R = 0.1$ and $Q = \text{diag}\{13, 14.5, 165, 0\}$, $R = 0.1$, respectively; the corresponding LQR controllers are derived by MATLAB as $M_{\text{lqr}} = -10(\phi - \phi_d) - 18.0514(\dot{\phi} - \dot{\phi}_d) + 24.4277\theta_2 + 5.82\dot{\theta}_2$, $F_{\text{lqr}} = -10(x - x_d) - 16.746(\dot{x} - \dot{x}_d) + 29.6098\theta_1 + 4.1224\dot{\theta}_1$ (which we call LQR 1) and $M_{\text{lqr}} = -11.4018(\phi - \phi_d) - 19.0151(\dot{\phi} - \dot{\phi}_d) + 26.4348\theta_2 + 5.9425\dot{\theta}_2$, $F_{\text{lqr}} = -11.4018(x - x_d) - 17.6068(\dot{x} - \dot{x}_d) + 31.7093\theta_1 + 4.1266\dot{\theta}_1$ (which we call LQR 2), respectively. After tuning, the control parameters for the designed controller (20) are selected as $k_{p\phi} = 26$, $k_{d\phi} = 3.1$, $k_{px} = 71.4$, $k_{dx} = 13$, $k_{hx} = 3.5$, $k_{h\phi} = 4.5$, $\beta_x = \beta_\phi = 0.01$, $\varepsilon_x = 0.002$, $\varepsilon_\phi = 0.003$, $\pi_{\phi 1} = 0.6$, $\pi_{\phi 2} = 0.8$, $\pi_{x1} = \pi_{x2} = 10$, $\hat{M}_{f1}(0) = \hat{M}_{f2}(0) = \hat{F}_{f1}(0) = \hat{F}_{f2}(0) = 0$. To better exhibit the experimental results, we introduce the following performance indices:

1) $\theta_{1\max}$, $\theta_{2\max}$: maximum swing amplitudes, i.e., $\theta_{1\max} \triangleq \max_t\{|\theta_1(t)|\}$, $\theta_{2\max} \triangleq \max_t\{|\theta_2(t)|\}$.
2) $\theta_{1\text{res}}$, $\theta_{2\text{res}}$: residual swing defined as the maximum swing amplitudes after 6 s, i.e., $\theta_{1\text{res}} \triangleq \max_{t\geq 6}\{|\theta_1(t)|\}$, $\theta_{2\text{res}} \triangleq \max_{t\geq 6}\{|\theta_2(t)|\}$.
3) $M_{\max}$, $F_{\max}$: maximum control force/torque amplitudes, i.e., $M_{\max} \triangleq \max_t\{|M(t)|\}$, $F_{\max} \triangleq \max_t\{|F(t)|\}$.

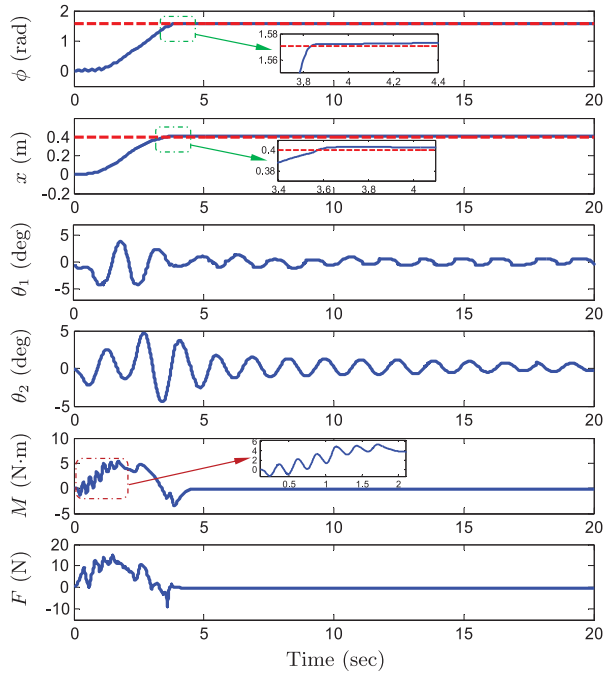

Fig. 3. Results for Experiment 1: the robust EI method in [44] (dashed lines: $\phi_d = \pi/2$ rad and $x_d = 0.4$ m).

The obtained experimental results are recorded by the curves in Figs. 3–6, and the corresponding quantified performance indices introduced above are provided in Table I. When implementing the three kinds of control methods, the trolley and the jib all arrive at the target positions within 6 s. It is seen that the proposed adaptive control approach (see Fig. 6) exhibits *superior* antiswing performance over the comparative EI and LQR methods (see Figs. 3–5), in terms of maximum swing amplitude suppression (see $\theta_{1\max}$ and $\theta_{2\max}$ in Table I) and residual swing elimination (refer to $\theta_{1\text{res}}$ and $\theta_{2\text{res}}$ in Table I). There is almost no residual swing for the proposed controller (20), while obvious residual swing is observed for the comparative approaches.

By observing the locally zoomed plots in Figs. 3–5, the jib slew and trolley translation positions exceed the target positions. By contrast, Fig. 6 verifies that the proposed controller (20) can effectively prevent the trolley and jib motion from going beyond the target positions (i.e., avoiding overshoots), which is beneficial for practical applications. By comparing the results of LQR 1 and LQR 2 in Figs. 4 and 5 and also Table I, one finds that although LQR 2 reduces the overshoots to some extent by

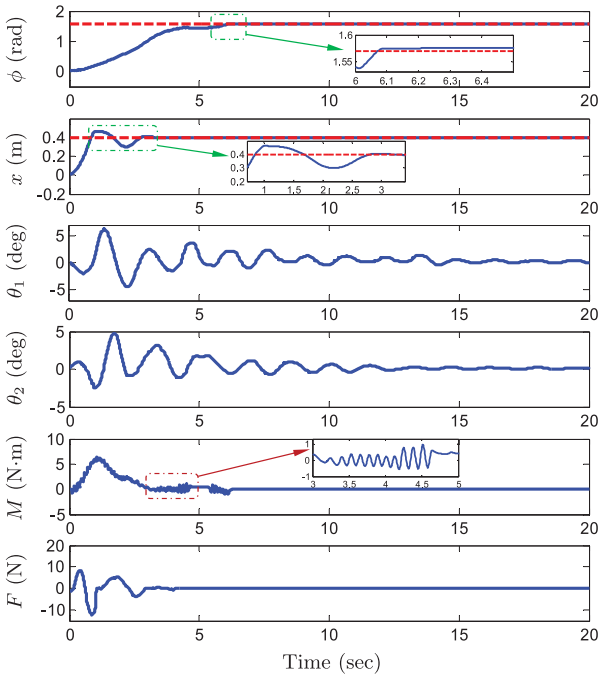

Fig. 4. Results for Experiment 1: LQR 1 (dashed lines: $\phi_d = \pi/2$ rad and $x_d = 0.4$ m).

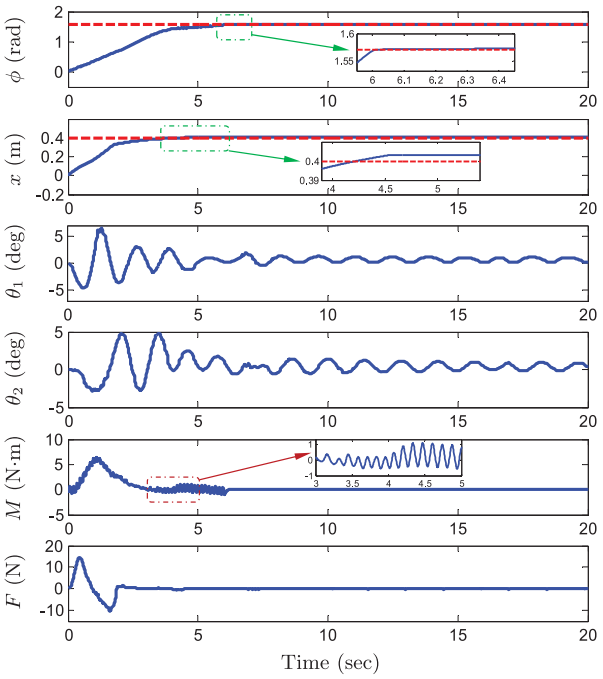

Fig. 5. Results for Experiment 1: LQR 2 (dashed lines: $\phi_d = \pi/2$ rad and $x_d = 0.4$ m).

adjusting the values of Q and R, it results in larger swing amplitudes and more significant residual swing as a tradeoff. Additionally, it is seen from the zoomed plots for $M(t)$ in Figs. 3–6 that the control input signals are a bit noisy. This is caused by the fact that the velocity signals are obtained by using the numerical difference technique together with low-pass filters, because

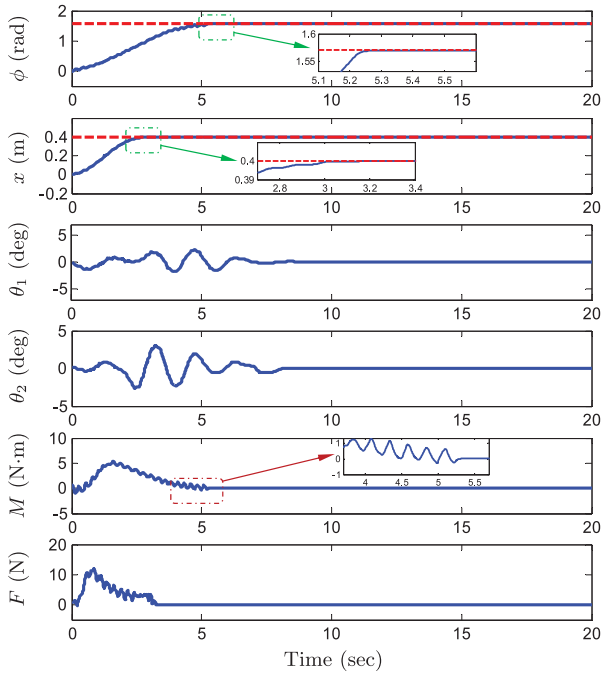

Fig. 6. Results for Experiment 1: the proposed control method (dashed lines: $\phi_d = \pi/2$ rad and $x_d = 0.4$ m).

TABLE I
PERFORMANCE INDICES OF EXPERIMENT 1

Methods	$\theta_{1\max}$ (degree)	$\theta_{2\max}$ (degree)	$\theta_{1\text{res}}$ (degree)	$\theta_{2\text{res}}$ (degree)	$M_{\max}$ (N · m)	$F_{\max}$ (N)
EI method	4.22	4.67	1.13	1.37	5.36	14.91
LQR 1	6.29	4.80	2.31	1.14	6.48	12.31
LQR 2	6.59	4.83	1.58	1.44	6.32	14.56
Proposed method	2.21	3.03	0.26	0.56	5.39	11.88

they are not directly measurable; then, there unavoidably exist unfiltered noises in the velocity signals, which are further incorporated into the control inputs. For practical implementation, if needed, one can further use low-pass filters to smooth the control signals, as commonly done in many mechatronic control systems.

2) Experiment 2: In order to further validate the robustness performance of the designed control method, we carry out experiments by considering the following cases.

1) *Case 1: Parametric uncertainties.* We change m_p and L to $m_p = 1$ kg and $L = 0.8$ m, respectively, while the nominal values are still regarded the same as in (56).
2) *Case 2: External perturbations and time-varying rope length.* The rope length is *online* changed from 0.4 m at $t = 0$ s to 0.6 m at $t = 5$ s with an average rate of 0.04 m/s. At the same time, external perturbations are exerted on the swing *on purpose* for three times at about 6.1, 8.6, and 13.1 s, respectively; see the marked parts in Fig. 8.
3) *Case 3: Initial swing angle disturbances.* We set the initial swing angles as $\theta_1(0) \approx -6.0^\circ$, $\theta_2(0) \approx -3.0^\circ$.

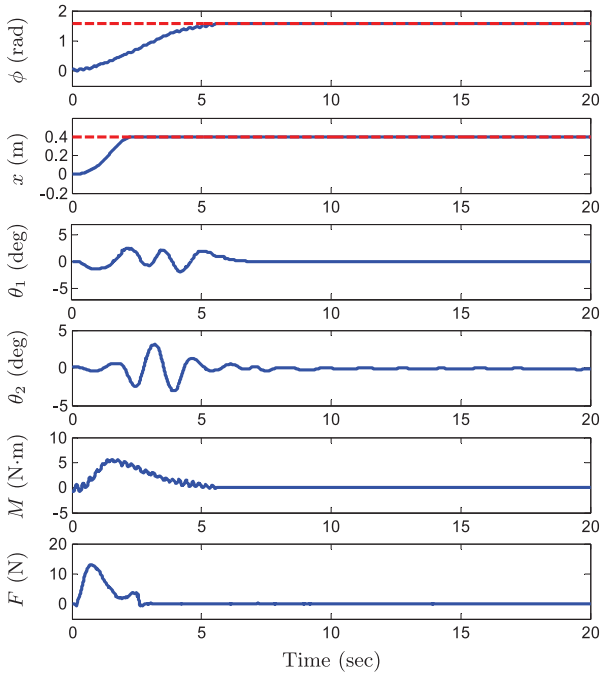

Fig. 7. Results for Experiment 2–Case 1: parametric uncertainties (dashed lines: $\phi_d = \pi/2$ rad and $x_d = 0.4$ m).

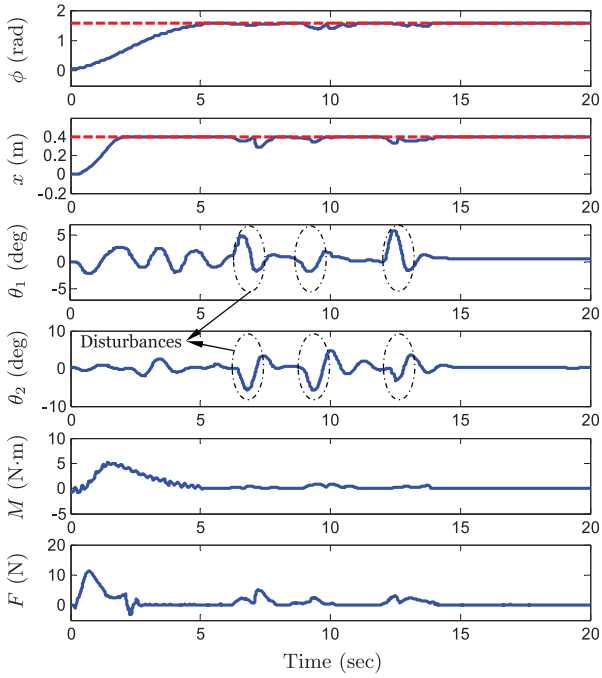

Fig. 8. Results for Experiment 2–Case 2: external perturbations and time-varying rope length (dashed lines: $\phi_d = \pi/2$ rad and $x_d = 0.4$ m).

For all the three cases, the proposed method's control parameters are selected the same with those used in *Experiment 1*. The curves in Figs. 7–9 depict the experimental results corresponding to the above three cases. It is seen, by comparing Figs. 6 with 7, that the overall performances of the presented control scheme in different system parameter settings are quite similar,

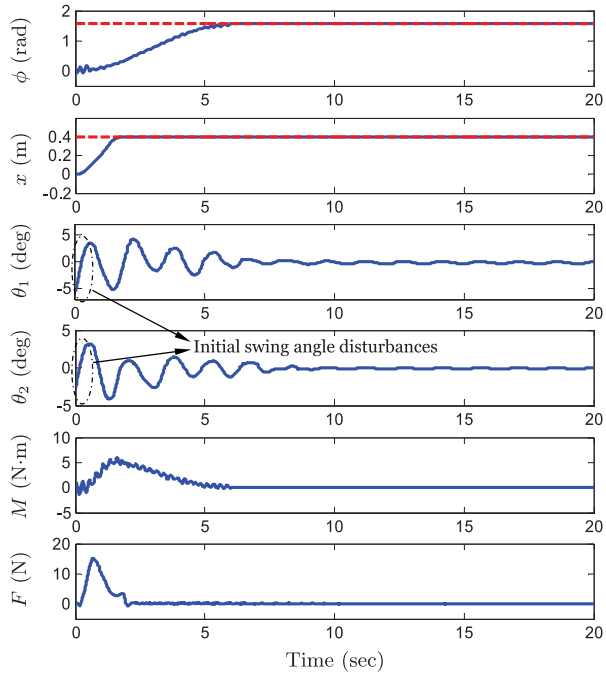

Fig. 9. Results for Experiment 2–Case 3: initial swing angle disturbances (dashed lines: $\phi_d = \pi/2$ rad and $x_d = 0.4$ m).

implying its satisfactory adaptability to parametric changes (uncertainties). Further, as shown in Fig. 8, one can find that the presented control method still performs satisfactorily even when the rope length is time-varying and unexpected extraneous perturbations are incorporated. Finally, we can observe from Fig. 9 that the designed method is insensitive to nonzero initial swing conditions. From the above analysis, it is evident that the presented method is effective for controlling underactuated tower cranes and shows satisfactory robustness.

VI. Conclusion

We have proposed a new adaptive control approach for tower crane systems, where parametric uncertainties are present. Compared with existing tower crane control methods, the proposed method has both theoretical and practical significance. In the theoretical aspect, the proposed approach does not need to linearize the tower crane dynamical equations around the equilibrium point or to neglect nonlinear terms, and rigorous theoretical analysis has been carried out based upon the full nonlinear dynamics. On the other hand, from the practical viewpoint, the proposed scheme achieves superior control performance over the comparative EI and LQR methods and shows good robustness, which has been verified by hardware experiments implemented on a self-built multifunctional crane testbed.

Acknowledgment

The authors would like to thank all the reviewers and the Associate Editor for their constructive suggestions and comments, which have greatly improved the quality of this paper.

REFERENCES

[1] E. M. Abdel-Rahman, A. H. Nayfeh, and Z. N. Masoud, "Dynamics and control of cranes: A review," *J. Vib. Control*, vol. 9, no. 7, pp. 863–908, Jul. 2003.

[2] Y. Tian and S. Li, "Exponential stabilization of nonholonomic dynamic systems by smooth time-varying control," *Automatica*, vol. 38, no. 7, pp. 1139–1146, Jul. 2002.

[3] S. Ding, S. Li, and Q. Li, "Global uniform asymptotical stability of a class of nonlinear cascaded systems with application to a nonholonomic wheeled mobile robot," *Int. J. Syst. Sci.*, vol. 41, no. 11, pp. 1301–1312, Nov. 2010.

[4] M. Ou, H. Du, and S. Li, "Finite-time formation control of multiple nonholonomicmobile robots," *Int. J. Robust Nonlinear Control*, vol. 24, no. 1, pp. 140–165, Jan. 2014.

[5] X. Zhang, B. Xian, B. Zhao, and Y. Zhang, "Autonomous flight control of a nano quadrotor helicopter in a GPS-denied environment using onboard vision," *IEEE Trans. Ind. Electron.*, vol. 62, no. 10, pp. 6392–6403, Oct. 2015.

[6] H. Sun, S. Li, and C. Sun, "Finite time integral sliding mode control of hypersonic vehicles," *Nonlinear Dyn.*, vol. 73, no. 1, pp. 229–244, Jul. 2013.

[7] S. Li and X. Wang, "Finite-time consensus and collision avoidance control algorithms for multiple AUVs," *Automatica*, vol. 49, no. 11, pp. 3359–3367, Nov. 2013.

[8] J.-X. Xu, Z.-Q. Guo, and T. H. Lee, "Design and implementation of integral sliding mode control on an underactuated two-wheeled mobile robot," *IEEE Trans. Ind. Electron.*, vol. 61, no. 7, pp. 3671–3681, Jul. 2014.

[9] D. Xia, L. Wang, and T. Chai, "Neural-network friction compensation based energy swing-up control of Pendubot," *IEEE Trans. Ind. Electron.*, vol. 61, no. 3, pp. 1411–1423, Mar. 2014.

[10] X.-Z. Lai, C.-Z. Pan, M. Wu, S. X. Yang, and W.-H. Cao, "Control of an underactuated three-link passive-active-active manipulator based on three stages and stability analysis," *J. Dyn. Syst, Meas. Control*, vol. 137, no. 2, pp. 021007-1–021007-9, Sep. 2014.

[11] X. Xin and Y. Liu, "Reduced-order stable controllers for two-link underactuated planar robots," *Automatica*, vol. 49, no. 7, pp. 2176–2183, Jul. 2013.

[12] Q. Zang and J. Huang, "Dynamics and control of three-dimensional slosh in a moving rectangular liquid container undergoing planar excitations," *IEEE Trans. Ind. Electron.*, vol. 62, no. 4, pp. 2309–2318, Apr. 2015.

[13] S. Li, J. Li, and Y. Mo, "Piezoelectric multimode vibration control for stiffened plate using ADRC-based acceleration compensation," *IEEE Trans. Ind. Electron.*, vol. 61, no. 12, pp. 6892–6902, Dec. 2014.

[14] K. Sorensen and W. Singhose, "Command-induced vibration analysis using input shaping principles," *Automatica*, vol. 44, no. 9, pp. 2392–2397, Sep. 2008.

[15] S. Garrido, M. Abderrahim, A. Giménez, R. Diez, and C. Balaguer, "Anti-swinging input shaping control of an automatic construction crane," *IEEE Trans. Autom. Sci. Eng.*, vol. 5, no. 3, pp. 549–557, Jul. 2008.

[16] N. Sun, Y. Fang, Y. Zhang, and B. Ma, "A novel kinematic coupling-based trajectory planning method for overhead cranes," *IEEE/ASME Trans. Mechatronics*, vol. 17, no. 1, pp. 166–173, Feb. 2012.

[17] R. Liu, S. Li, and S. Ding, "Nested saturation control for overhead crane systems," *Trans. Instrum. Meas. Control*, vol. 34, no. 7, pp. 862–875, Oct. 2012.

[18] R. Liu and S. Li, "Suboptimal integral sliding mode controller design for a class of affine systems," *J. Optim. Theory Appl.*, vol. 161, no. 3, pp. 877–904, Jun. 2014.

[19] N. Sun, Y. Fang, and H. Chen, "A new antiswing control method for underactuated cranes with unmodeled uncertainties: Theoretical design and hardware experiments," *IEEE Trans. Ind. Electron.*, vol. 62, no. 1, pp. 453–465, Jan. 2015.

[20] C. Vázquez, J. Collado, and L. Fridman, "Control of a parametrically excited crane: A vector Lyapunov approach," *IEEE Trans. Control Syst. Technol.*, vol. 21, no. 6, pp. 2332–2340, Nov. 2013.

[21] N. Sun and Y. Fang, "Nonlinear tracking control of underactuated cranes with load transferring and lowering: Theory and experimentation," *Automatica*, vol. 50. no. 9, pp. 2350–2357, Sep. 2014.

[22] N. Sun, Y. Fang, and X. Zhang, "Energy coupling output feedback control of 4-DOF underactuated cranes with saturated inputs," *Automatica*, vol. 49, no. 5, pp. 1318–1325, May 2013.

[23] N. Sun and Y. Fang, "New energy analytical results for the regulation of underactuated overhead cranes: An end-effector motion-based approach," *IEEE Trans. Ind. Electron.*, vol. 59, no. 12, pp. 4723–4734, Dec. 2012.

[24] H. Lee, "Motion planning for three-dimensional overhead cranes with high-speed load hoisting," *Int. J. Control*, vol. 78, no. 12, pp. 875–886, Aug. 2005.

[25] T. A. Le, S.-G. Lee, and S.-C. Moon, "Partial feedback linearization and sliding mode techniques for 2D crane control," *Trans. Inst. Meas. Control*, vol. 36, no. 1, pp. 78–87, Feb. 2014.

[26] H. Park, D. Chwa, and K.-S. Hong, "A feedback linearization control of container cranes: Varying rope length," *Int. J. Control, Autom., Syst.*, vol. 5, no. 4, pp. 379–387, Aug. 2007.

[27] K. Zavari, G. Pipeleers, and J. Swevers, "Gain-scheduled controller design: Illustration on an overhead crane," *IEEE Trans. Ind. Electron.*, vol. 61, no. 7, pp. 3713–3718, Jul. 2014.

[28] G. Boschetti, R. Caracciolo, D. Richiedei, and A. Trevisani, "Moving the suspended load of an overhead crane along a pre-specified path: A non-time based approach," *Robot. Comput.-Integr. Manuf.*, vol. 30, no. 3, pp. 256–264, Jun. 2014.

[29] N. Uchiyama, "Robust control for overhead cranes by partial state feedback," *Proc. Inst. Mech. Eng. I, J. Syst. Control Eng.*, vol. 223, no. 4, pp. 575–580, Jun. 2009.

[30] N. Sun, Y. Fang, H. Chen, and B. He, "Adaptive nonlinear crane control with load hoisting/lowering and unknown parameters: Design and experiments," *IEEE/ASME Trans. Mechatronics*, vol. 20, no. 5, pp. 2107–2119, Oct. 2015.

[31] W. He, S. Zhang, and S. S. Ge, "Adaptive control of a flexible crane system with the boundary output constraint," *IEEE Trans. Ind. Electron.*, vol. 61, no. 8, pp. 4126–4133, Aug. 2014.

[32] D. Liu, J. Yi, D. Zhao, and W. Wang, "Adaptive sliding mode fuzzy control for a two-dimensional overhead crane," *Mechatronics*, vol. 15, no. 5, pp. 505–522, Jun. 2005.

[33] W. Chen and M. Saif, "Output feedback controller design for a class of MIMO nonlinear systems using high-order sliding-mode differentiators with application to a laboratory 3-D crane," *IEEE Trans. Ind. Electron.*, vol. 55, no. 11, pp. 3985–3996, Nov. 2008.

[34] T. Kaneko, H. Mine, and K. Ohishi, "Anti sway crane control based on sway angle observer with sensor-delay correction," *IEEJ Trans. Ind. Appl.*, vol. 129, no. 6, pp. 555–563, Jun. 2009.

[35] L.-H. Lee, C.-H. Huang, S.-C. Ku, Z.-H. Yang, and C.-Y. Chang, "Efficient visual feedback method to control a three-dimensional overhead crane," *IEEE Trans. Ind. Electron.*, vol. 61, no. 8, pp. 4073–4083, Aug. 2014.

[36] Y. Zhao and H. Gao, "Fuzzy-model-based control of an overhead crane with input delay and actuator saturation," *IEEE Trans. Fuzzy Syst.*, vol. 20, no. 1, pp. 181–186, Feb. 2012.

[37] W. Yu, M. A. Moreno-Armendariz, and F. O. Rodriguez, "Stable adaptive compensation with fuzzy CMAC for an overhead crane," *Inf. Sci.*, vol. 181, no. 21, pp. 4895–4907, Nov. 2011.

[38] K. Nakazono, K. Ohnishi, H. Kinjo, and T. Yamamoto, "Load swing suppression for rotary crane system using direct gradient descent controller optimized by genetic algorithm," *Trans. Inst. Syst., Control Inf. Eng.*, vol. 22, no. 8, pp. 303–310, Aug. 2011.

[39] F. Ju, Y. S. Choo, and F. S. Cui, "Dynamic response of tower crane induced by the pendulum motion of the payload," *Int. J. Solids Struct.*, vol. 43, no. 2, pp. 376–389, Jan. 2006.

[40] H. M. Omar and A. H. Nayfeh, "Gain scheduling feedback control for tower cranes," *J. Vib. Control*, vol. 9, no. 3-4, pp. 399–418, Mar./Apr. 2003.

[41] H. M. Omar and A. H. Nayfeh, "Gain scheduling feedback control of tower cranes with friction compensation," *J. Vib. Control*, vol. 10, no. 2, pp. 269–289, Feb. 2004.

[42] G. Lee *et al.*, "A laser-technology-based lifting-path tracking system for a robotic tower crane," *Autom. Construction*, vol. 18, no. 7, pp. 865–874, Nov. 2009.

[43] J. Vaughan, D. Kim, and W. Singhose, "Control of tower cranes with double-pendulum payload dynamics," *IEEE Trans. Control Syst. Technol.*, vol. 18, no. 6, pp. 1345–1358, Nov. 2010.

[44] J. Vaughan, A. Yano, and W. Singhose, "Comparison of robust input shapers," *J. Sound Vib.*, vol. 315, nos. 4/5, pp. 797–815, Sep. 2008.

[45] Y. Maeda, M. Wada, M. Iwasaki, and H. Hirai, "Improvement of settling performance by mode-switching control with split initial-value compensation based on input shaper," *IEEE Trans. Ind. Electron.*, vol. 60, no. 3, pp. 979–987, Mar. 2013.

[46] W. Devesse, M. Ramteen, L. Feng, and J. Wikander, "A real-time optimal control method for swing-free tower crane motions," in *Proc. IEEE Int. Conf. Autom. Sci. Eng.*, Madison, WI, USA, Aug. 2013, pp. 336–341.
[47] M. Böck and A. Kugi, "Real-time nonlinear model predictive path-following control of a laboratory tower crane," *IEEE Trans. Control Syst. Technol.*, vol. 22, no. 4, pp. 1461–1473, Jul. 2014.
[48] S. C. Duong, E. Uezato, H. Kinjo, and T. Yamamoto, "A hybrid evolutionary algorithm for recurrent neural network control of a three-dimensional tower crane," *Autom. Construction*, vol. 23, pp. 55–63, May 2012.
[49] W.-H. Chen, D. J. Ballance, P. J. Gawthrop, and J. O'Reilly, "A nonlinear disturbance observer for robotic manipulators," *IEEE Trans. Ind. Electron.*, vol. 47, no. 4, pp. 932–938, Apr. 2000.
[50] J. Yang, S. Li, and X. Yu, "Sliding-mode control for systems with mismatched uncertainties via a disturbance observer," *IEEE Trans. Ind. Electron.*, vol. 60, no. 1, pp. 160–169, Jan. 2013.
[51] J. Yang, J. Su, S. Li, and X. Yu, "High-order mismatched disturbance compensation for motion control systems via a continuous dynamic sliding-mode approach," *IEEE Trans. Ind. Informat.*, vol. 10, no. 1, pp. 604–614, Feb. 2014.
[52] H. K. Khalil, *Nonlinear Systems*, 3rd ed. Englewood Cliffs, NJ, USA: Prentice-Hall, 2002.

Ning Sun (S'12–M'14) received the B.S. degree in measurement and control technology and instruments (Hons.) from Wuhan University, Wuhan, China, in 2009, and the Ph.D. degree in control theory and control engineering (Hons.) from Nankai University, Tianjin, China, in 2014.

He is currently with the Institute of Robotics and Automatic Information Systems, Nankai University. His research interests include cranes, wheeled robots, and nonlinear control with applications to mechatronic systems.

Dr. Sun is a Member of the IEEE Industrial Electronics Society Technical Committee on Control, Robotics, and Mechatronics and a Program Committee Member for several international conferences. He received the Nomination Award of the Guan Zhao-Zhi Best Paper Award at the 32nd Chinese Control Conference.

Yongchun Fang (S'00–M'02–SM'08) received the B.S. and M.S. degrees in control theory and applications from Zhejiang University, Hangzhou, China, in 1996 and 1999, respectively, and the Ph.D. degree in electrical engineering from Clemson University, Clemson, SC, USA, in 2002.

From 2002 to 2003, he was a Postdoctoral Fellow with the Sibley School of Mechanical and Aerospace Engineering, Cornell University, Ithaca, NY, USA. He is currently a Professor with the Institute of Robotics and Automatic Information Systems, Nankai University, Tianjin, China. His research interests include nonlinear control, visual servoing, control of underactuated systems, and AFM-based nano-systems.

Prof. Fang is an Associate Editor of the *ASME Journal of Dynamic Systems, Measurement, and Control* and *Control Theory and Applications*.

He Chen received the B.S. degree in automation from Nankai University, Tianjin, China, in 2013, where he is currently working toward the Ph.D. degree in control theory and control engineering in the Institute of Robotics and Automatic Information Systems.

His research interests include control of mechatronics, overhead cranes, and wheeled mobile robots.

Biao Lu received the B.S. degree in intelligence science and technology from Nankai University, Tianjin, China, in 2015, where he is currently working toward the Ph.D. degree in control theory and control engineering in the Institute of Robotics and Automatic Information Systems.

His research interests include control of overhead cranes and offshore cranes.

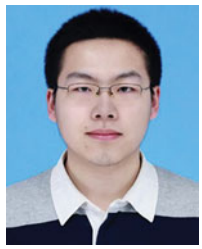

Yiming Fu received the B.S. degree in intelligence science and technology from Nankai University, Tianjin, China, in 2013, where he is currently working toward the M.S. degree in control theory and control engineering in the Institute of Robotics and Automatic Information Systems.

His research interests include control of underactuated overhead cranes and offshore cranes.